Landau-Zener Transition in the Dynamic Transfer of Acoustic Topological States

Ze-Guo Chen,[1] Weiyuan Tang,[1] Ruo-Yang Zhang,[2] Zhaoxian Chen,[3] and Guancong Ma[1,*]
[1]Department of Physics, Hong Kong Baptist University, Kowloon Tong, Hong Kong, China
[2]Department of Physics, The Hong Kong University of Science and Technology, Clear Water Bay, Hong Kong, China
[3]Department of Physics, Nanjing University, Nanjing 210093, People's Republic of China

(Received 3 August 2020; accepted 21 December 2020; published 1 February 2021)

Topological notions in physics often emerge from adiabatic evolution of states. It not only leads to fundamental insight of topological protection but also provides an important approach for the study of higher-dimensional topological phases. In this work, we first demonstrate the transfer of topological boundary states (TBSs) across the bulk to the opposite boundary in an acoustic waveguide system. By exploring the finite-size induced minigap between two TBS bands, we unveil the quantitative condition for the breakdown of adiabaticity in the system by demonstrating the Landau-Zener transition with both theory and experiments. Our results not only serve as a foundation of future studies of dynamic state transfer but also inspire applications leveraging nonadiabatic transitions as a new degree of freedom.

DOI: 10.1103/PhysRevLett.126.054301

The emergence of topological effects in physics is often underlain by adiabatic cyclic variation of a specific set of parameters, which leads to quantized Berry phases that give rise to various types of topological invariants [1,2]. Perhaps the best-known example is a Chern insulator, which is characterized by a topological invariant known as the TKNN number (or in many cases, the Chern number) [3]. Underpinned by the fundamental universality of topology, recent efforts have identified that similar physical phenomena not only exist in solid-state electronic systems but also in photonics and electromagnetism [4,5], elastics, and acoustics [6,7].

Thouless pumping is another important manifestation of topology in physics [8,9]. It is regarded as a dynamical version of the two-dimensional (2D) quantum Hall effect [10–14]. Recent observations of Thouless pumping in optical lattice [15–17], photonic waveguide arrays [18–21], and elastic plates [14,22] show that dynamic evolution not only reveals topological insights of state evolution but also is a powerful method for studying higher-dimensional topological physics [19,23]. However, the robust dynamic pumping requires adiabatic variation of phase-space parameters. Deviation from adiabatic conditions will inevitably cause undesired states to be populated, and eventually the breakdown of the outcome [24]. However, despite its fundamental importance, nonadiabatic transition in topologically related phenomena remains largely unexplored so far.

In this Letter, we present a theoretical and experimental study of nonadiabatic transition in the dynamic evolution of acoustic topological boundary states (TBSs) in a commensurate Harper model [25]. Two TBSs localized at opposite boundaries can evanescently couple in a finite-sized system in the formation of a minigap [26], which we exploit for the investigation of the breakdown of adiabaticity. We show that such a breakdown follows the Landau-Zener model [27–29], wherein the adiabatic condition is linked to the rate of parameter modulation as well as the size of the TBS gap. Our work also presents the successful realization of the TBS transfer, which has not yet been achieved for sound waves. The results also offer insights to applications relying on the adiabatic evolution of states and open nonadiabatic transitions as a new degree of freedom for controlling the propagation of classical waves.

We consider a finite chain shown in Fig. 1(a), described by a commensurate Harper model [25]

$$H(\phi) = \sum_{m}^{N} [f_0 + \sigma\lambda\cos(2\pi bm + \phi)]|m\rangle\langle m| + \sum_{m}^{N-1} t|m\rangle\langle m+1| + \text{H.c.}, \quad (1)$$

where m labels the sites, t is the hopping coefficient, N is the total number of sites in the finite chain, $\sigma = \pm 1$ is a degree of freedom. The onsite terms are periodically modulated as $f_0 + \sigma\lambda\cos(2\pi bm + \phi)$. Here, λ is the modulation amplitude and $b = \frac{1}{3}$ is the modulation frequency, and the parameter ϕ serves as a synthetic dimension of the system. Two eigenspectra are plotted as functions of ϕ, two band gaps are bridged by two chiral TBSs that are protected by nontrivial Chern number C computed in the $k\phi$ plane, as shown in Fig. 1(b). The relative locations of the two TBSs on the ϕ axis are drastically different, depending on the total site number N. When $N = 3n$ with n being an integer, the two TBSs intersect, and a minigap is opened due to a finite-sized effect of the chain (left panel) [30]. But if $N = 3n - 1$, the

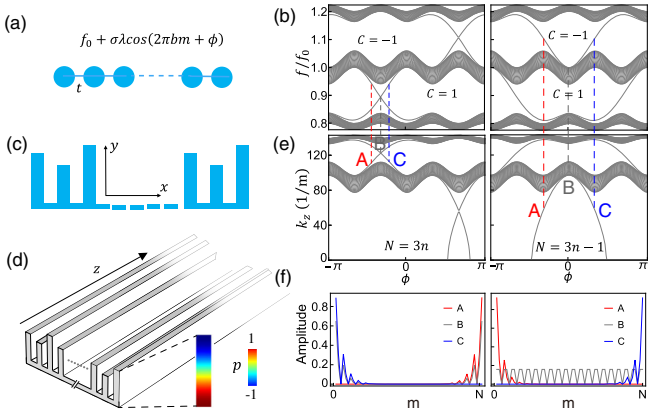

FIG. 1. (a) A schematic of a finite Harper chain. The onsite frequency is periodically modulated. (b) The calculated eigenspectra as functions of ϕ. The parameters are $f_0 = 9101.5$ Hz, $t = -0.082 f_0$, $\lambda = -2t$. The left (right) panel corresponds to a chain with $N = 60$ (59) sites and $\sigma = -1(+1)$. (c),(d) Schematics of an acoustic waveguide array for realizing the finite Harper chain. The color map in (d) shows the cross-sectional profile of the guiding mode. (e) The calculated eigenspectra of the Hamiltonian in Eq. (2), in which the eigenvalues are the propagation constant k_z. The states at A, B, and C in (e) are shown in (f).

two TBSs are symmetric about $\phi = 0$. This can be seen by a unitary transformation that flips the sign of ϕ: $H(\phi) = P^{-1}H(-\phi)P$, where P is a unitary operator with $P_{ij} = 1$ for $i + j = N + 1$.

The Harper model can be realized using coupled acoustic cavities [31,32], which can be extended to a waveguide array [33,34], as schematically shown in Figs. 1(c) and 1(d). The system consists of N rectangular air-filled waveguides coupled by a thin sheet of air. The cross section of the array reproduces the Harper model [Eq. (1)] with a specific ϕ. Here, we employ the first-order guiding mode [Fig. 1(d)], denoted $|\psi_j(\phi)\rangle e^{ik_z z}$, where $|\psi_j(\phi)\rangle$ is an eigenfunction of $H(\phi)$ with a corresponding eigenfrequency $f_{H,j}(\phi)$, with j labeling the bands. When the working frequency is fixed at f_w, the propagation constant is $k_{z,j}(\phi) = (2\pi/c)\sqrt{f_w^2 - f_{H,j}^2(\phi)}$, where c is the speed of sound. Equation (1) can then be transformed to

$$\mathcal{H}(\phi) = \Psi K_z \Psi^{\dagger}. \tag{2}$$

Here $\Psi = (|\psi_1(\phi)\rangle, |\psi_2(\phi)\rangle \ldots |\psi_N(\phi)\rangle)$, is a column matrix formed by all eigenvectors of $H(\phi)$; $K_z = \sum_j^N k_{z,j}(\phi)|j\rangle\langle j|$. Equation (2) shares the same set of eigenfunctions as Eq. (1), but the corresponding eigenvalues become $k_{z,j}$, as shown in Fig. 1(e). It follows that ϕ directly links to k_z. We can then enforce the adiabatic variation of ϕ by slowly modulating the waveguide along the z direction [35]:

$$-i\partial_z|\psi(z)\rangle = \mathscr{H}(z)|\psi(z)\rangle, \tag{3}$$

which is a Schrödinger-type equation. Since the first-order guiding mode resembles a dipole in its cross-sectional profile [Fig. 1(d)], the adiabatic variation of ϕ, which affects the onsite frequency [Eq. (1)], can be implemented by a continuous change of the height of each waveguide, as schematically shown in Fig. 2(a).

Changing the total number of waveguides N leads to entirely different state transfer processes, as shown in Figs. 1(b)–1(f). With $N = 3n - 1$, the transfer of the TBS to the opposite boundary must connect through a bulk band near $\phi = 0$ or π. This implies that ϕ must be driven across a rather large range to achieve well-localized TBS as end states [35]. On the contrary, when $N = 3n$, the TBS bands intersect at $\phi = -\pi/3$ (in the lower gap). In a finite-size system, these TBSs couple evanescently and a small gap opens near the crossing points [30]. In this case, the TBS can transfer to the opposite boundary without involving any bulk states, as shown in Fig. 1(f). It also has the advantage of requiring the variation of a much smaller range of ϕ. However, as we will demonstrate next, the small size of the TBS gap means that such an effect is sensitive to the condition of adiabaticity and therefore offers a unique opportunity for studying nonadiabatic transition.

We investigate a nine-waveguide array whose height is modulated according to $h_m = 20 + 5\cos(2m\pi/3 + \phi)$ mm [Fig. 2(a)]. The hopping is achieved by air layer with a thickness $w = 3$ mm, which is chosen to generate a properly sized TBS gap. The two waveguides at the boundaries have an additional height correction of

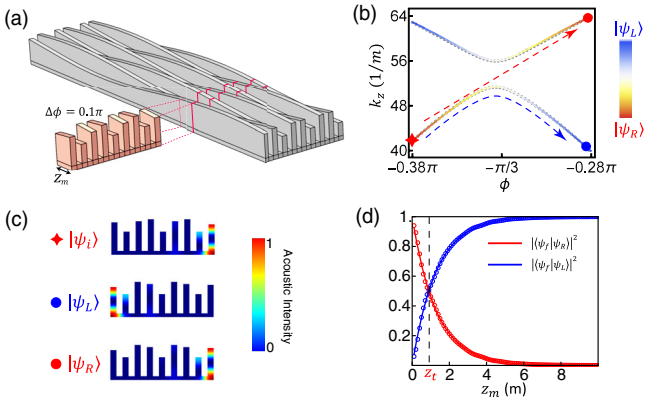

FIG. 2. (a) A schematic drawing of the acoustic waveguide array with modulated height. The modulation range is shown by the red section. (b) Propagation constant k_z as a function of ϕ near $\phi = -\pi/3$ at a working frequency $f_w = 9.5$ kHz. The solid curves (dots) are results based on the two-band model (finite-element simulations). (c) The field distribution of the initial state (star) and the two possible final states (circles). (d) The weighting of left and right TBSs as functions of modulation length z_m. The solid curves are the direct results of the Landau-Zener model, and the open circles are from numerical simulations.

$\Delta h = -2$ mm to compensate for the perturbation to onsite frequency induced by the coupling [32]. Mode analysis using COMSOL Multiphysics at a working frequency $f_w = 9.5$ kHz reveals that the TBS gap has a size of $\Delta k_z = 4.66\ \mathrm{m}^{-1}$, as shown Fig. 2(b). In the vicinity of $\phi = -\pi/3$, the TBS gap can be modeled by a two-level effective Hamiltonian near $k_z = 53.7\ \mathrm{m}^{-1}$,

$$H_e(\delta\phi) = \begin{pmatrix} -\alpha\delta\phi & \Gamma \\ \Gamma & \alpha\delta\phi \end{pmatrix}. \tag{4}$$

Here, $\Gamma = \Delta k_z/2$ is determined by the gap size and $\alpha = 70.4\ \mathrm{m}^{-1}$ is a fitting parameter. The bases of H_e are $|\psi_L\rangle$ and $|\psi_R\rangle$, i.e., the TBSs localized at the left and right boundaries, respectively. The eigenvalues of H_e are plotted as the solid curves in Fig. 2(b), which are in excellent agreement with the results from mode analysis (dots). The weightings of $|\psi_L\rangle$ and $|\psi_R\rangle$ are shown by the blue and red colors. The initial state is $|\psi_R\rangle$ at $\phi = -0.38\pi$ (marked by the red star). The final state $|\psi_f\rangle$ is a combination of two boundary states $|\psi_R\rangle$ and $|\psi_L\rangle$. The two possible routes of state evolution across the TBS gap are represented by the dashed arrows in Fig. 2(b). When it follows the red path, $|\psi_R\rangle$, component dominates during the TBS transfer process, and the final state remains localized on the right boundary [Fig. 2(c)]. Alternatively, when it is pumped along the blue path, the $|\psi_L\rangle$ component dominates the final state, which induces field localization on the left boundary [Fig. 2(c)].

The composition of the final state can be predicted by the Landau-Zener model [27,36], which depends on the TBS gap size Δk_z and the rate of parameter evolution. In our system, the gap size is apparently fixed. The evolution rate $\Delta\phi/z_m$ is determined by, i.e., the ratio of the parameter range $\Delta\phi = 0.1\pi$ and the length of the modulated waveguides z_m [the red section in Fig. 2(a)]. Then the composition of the final state is given by $|\psi_f\rangle = L(z)|\psi_L\rangle + R(z)|\psi_R\rangle$, with $L(z)$ and $R(z)$ satisfying

$$-i\frac{d}{dz}\begin{pmatrix} L(z) \\ R(z) \end{pmatrix} = \begin{pmatrix} \beta z & \Gamma \\ \Gamma & -\beta z \end{pmatrix}\begin{pmatrix} L(z) \\ R(z) \end{pmatrix}, \tag{5}$$

where $\beta = \alpha(\Delta\phi/z_m)$ characterizes the adiabaticity. The state transfer begins with the state dominantly at $|\psi_R\rangle$ so that the initial condition is $(0, 1)^T$. From Eq. (5), we can work out the final state as a function of z_m, i.e., $R^2(z_m) = e^{-\pi\Gamma^2/\beta}$ and $L^2(z_m) = 1 - e^{-\pi\Gamma^2/\beta}$. We plot the final state weighting in Fig. 2(d) as functions of z_m. It is seen that $R^2(z_m)$ and $L^2(z_m)$ cross at $z_t = \frac{\alpha\Delta\phi \ln 2}{\pi\Gamma^2} = 0.899$ m. We denote this to be the transition point. The physics behind can be understood straightforwardly. With a fixed $\Delta\phi$, the length of waveguides determines the variation rate. When $z_m \gg z_t$, i.e., the waveguide array is long so that the state evolution is sufficiently slow to be adiabatic and the state remains on the same band. However, when the same process is enforced with a waveguide array shorter than z_t, the variation is fast so that adiabaticity is not satisfied. Then the upper TBS band is considerably populated, and the final state has a large component of $|\psi_R\rangle$. Hence we reach the conclusion that the energy of the final state redistributes according to the total length of modulation z_m [35].

We simulate four configurations to verify our analytical predictions. The numerical model is schematically shown in Fig. 3(a), in which a perfectly matched layer is used to eliminate reflection at the output. (In the experiments, the output is an open end that generates some reflection. However, this does not affect the state transfer results owing to the reciprocity of our system. See more

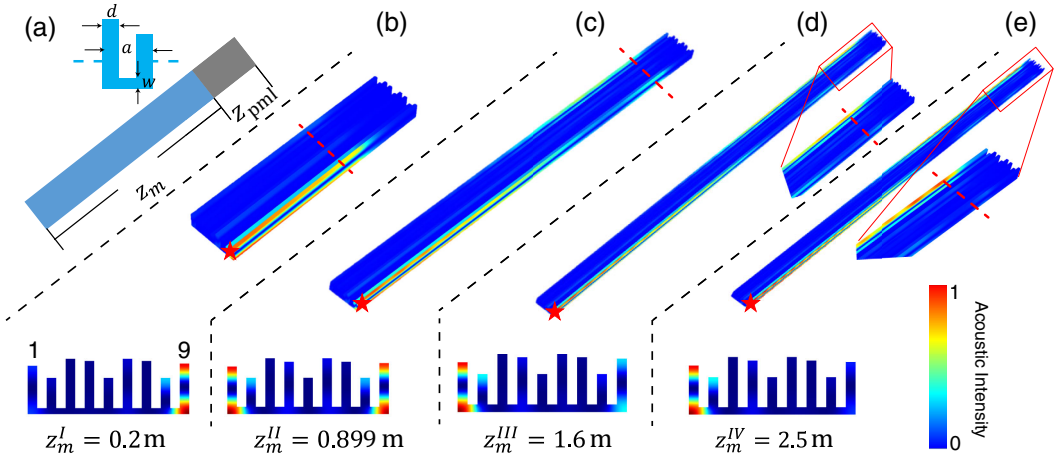

FIG. 3. (a) The model used in finite-element simulations. The parameters are $d = 4$, $w = 3$, and $a = 8$ mm. Perfectly matched layers with a length $z_{\mathrm{pml}} = 0.1$ m are added to the output ends to eliminate the reflection. (b)–(d) Simulation results for configuration I (b), II (c), III (d), IV (e). The red stars mark the source locations.

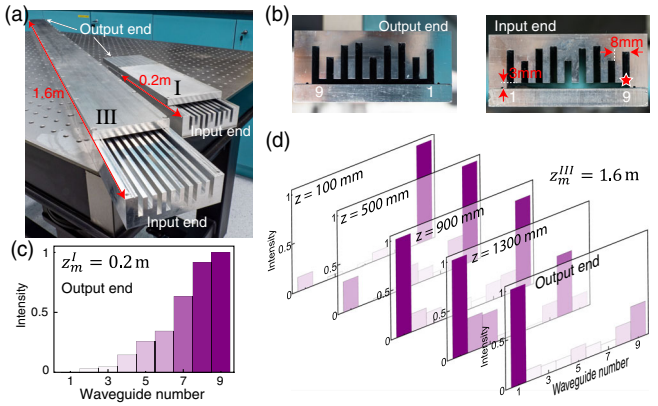

FIG. 4. (a) A photograph of the experimental acoustic waveguide arrays for configurations I and III. (b) Photographs of the input and output ends. (c) The measured acoustic intensity distribution at the output port for configuration I. (d) The measured TBS distributions along the axis in configuration III. Most acoustic energy is gradually transferred to waveguide 1, and no bulk state is excited in the process.

discussions in the Supplemental Material [35]). The simulated result of configuration I ($z_m^{\mathrm{I}} = 0.2$ m), shows that the initial and final states are both a TBS localized at the same boundary. For configuration II ($z_m^{\mathrm{II}} = 0.899$ m), the result [$L^2(z_m) = 0.54$] shows an almost equal distribution of acoustic energy at the left and right boundaries. For configuration III ($z_m^{\mathrm{III}} = 1.6$ m), most acoustic energy in the final state is localized at the left boundary. Further increase of z_m leads to the domination of $|\psi_R\rangle$ in the final state. These results shown in Figs. 3(b)–3(e) tally well with the theory. It is also noteworthy that in configurations II, III, and IV, the energy indeed is tunneled through the bulk to excite the left TBS without involving any bulk states, which is anticipated in our analysis. We remark that the avoidance of bulk states potentially makes the TBS transfer process more resilient against imperfections and loss [18].

We have verified these findings in experiments. Two configurations of waveguide arrays with different modulation lengths: $z_m^{\mathrm{I}} = 0.2$ and $z_m^{\mathrm{III}} = 1.6$ m were fabricated, as shown in Fig. 4(a). The acoustic waveguide arrays were precision machined from a block of aluminum. Frequency scan covering 9.5–9.7 kHz with a 2-Hz interval was performed by using a waveform generator (Keysight 33500B) that generates two antiphase sinusoidal signals to drive two identical loudspeakers (Hivi TN25) through audio power amplifiers. The loudspeakers formed a dipole source and were connected to waveguide 9 at the input. We then used a 3 mm microphone (RS-PRO 780-0734) to measure the acoustic responses in all waveguides. The data are recorded by a digital oscilloscope (Keysight DSO2024A). For each waveguide, we measured both the amplitude and phase at the top and the bottom and extracted the dipole component. For configuration I with $z_m^I < z_t$, the output profile shows that final state is dominantly $|\psi_R\rangle$ [Fig. 4(c)]. The results of configuration III with $z_m^{\mathrm{III}} > z_t$ are shown in Fig. 4(d). We have measured acoustic intensity distributions at different locations. It is clearly observed that the acoustic energy localizes at waveguide 9 near the input, and gradually transfer across the bulk to waveguide 1 at the output end. Also, the acoustic fields in the bulk region remain at a very low amplitude throughout the TBS transfer process, indicating that no bulk state is involved, which conforms well with our prediction. Note that due to the presence of dissipation, the results are normalized at different lengths. The constraints in both fabrication capability and laboratory space prevent the experiments on even longer waveguides. Nevertheless, our results already demonstrate the successful transfer of TBS and the nonadiabatic transition that follows the Landau-Zener model.

In summary, we have successfully demonstrated the transfer of TBSs in acoustics. Leveraging this acoustic system, we quantitatively identified the nonadiabatic transition condition, which could lead to the reliable control of adiabaticity that benefits the investigation of topological phenomena by dynamic processes. Our approach can be extended to higher dimensions and can benefit other physical systems, such as mechanical vibrations, electromagnetism, and electrical circuitries. Our work also shows that nonadiabatic transition can be exploited as a new degree of freedom for wave manipulations in topological and nontopological systems, which can open new application potentials such as the Landau-Zener-Stückelberg interferometry [37], asymmetric guiding mode switching [38], wave splitting, multiplexing, and demultiplexing of waveguide channels [39].

The authors thank C. T. Chan, Zhao-Qing Zhang, and Weiwei Zhu for helpful discussions. This work was supported by Hong Kong Research Grants Council (GRF 12302420, 12300419, ECS 22302718, CRF C6013-18G), National Science Foundation of China Excellent Young Scientist Scheme (Hong Kong and Macau) (No. 11922416) and Youth Program (No. 11802256), and Hong Kong Baptist University (RC-SGT2/18-19/SCI/006).

*Corresponding author.
phgcma@hkbu.edu.hk

[1] M. Z. Hasan and C. L. Kane, Rev. Mod. Phys. **82**, 3045 (2010).
[2] X.-L. Qi and S.-C. Zhang, Rev. Mod. Phys. **83**, 1057 (2011).
[3] D. J. Thouless, M. Kohmoto, M. P. Nightingale, and M. den Nijs, Phys. Rev. Lett. **49**, 405 (1982).
[4] L. Lu, J. D. Joannopoulos, and M. Soljacic, Nat. Photonics **8**, 821 (2014).
[5] T. Ozawa *et al.*, Rev. Mod. Phys. **91**, 015006 (2019).
[6] G. Ma, M. Xiao, and C. T. Chan, Nat. Rev. Phys. **1**, 281 (2019).

[7] X. Zhang, M. Xiao, Y. Cheng, M.-H. Lu, and J. Christensen, Commun. Phys. **1**, 97 (2018).
[8] D. J. Thouless, Phys. Rev. B **27**, 6083 (1983).
[9] L. J. Geerligs, V. F. Anderegg, P. A. M. Holweg, J. E. Mooij, H. Pothier, D. Esteve, C. Urbina, and M. H. Devoret, Phys. Rev. Lett. **64**, 2691 (1990).
[10] H.-Q. Zhou, S. Y. Cho, and R. H. McKenzie, Phys. Rev. Lett. **91**, 186803 (2003).
[11] L. Wang, M. Troyer, and X. Dai, Phys. Rev. Lett. **111**, 026802 (2013).
[12] I. H. Grinberg, M. Lin, C. Harris, W. A. Benalcazar, C. W. Peterson, T. L. Hughes, and G. Bahl, Nat. Commun. **11**, 974 (2020).
[13] X. Ni, K. Chen, M. Weiner, D. J. Apigo, C. Prodan, A. Alù, E. Prodan, and A. B. Khanikaev, Commun. Phys. **2**, 55 (2019).
[14] M. I. N. Rosa, R. K. Pal, J. R. F. Arruda, and M. Ruzzene, Phys. Rev. Lett. **123**, 034301 (2019).
[15] S. Nakajima, T. Tomita, S. Taie, T. Ichinose, H. Ozawa, L. Wang, M. Troyer, and Y. Takahashi, Nat. Phys. **12**, 296 (2016).
[16] M. Lohse, C. Schweizer, O. Zilberberg, M. Aidelsburger, and I. Bloch, Nat. Phys. **12**, 350 (2016).
[17] W. Ma, L. Zhou, Q. Zhang, M. Li, C. Cheng, J. Geng, X. Rong, F. Shi, J. Gong, and J. Du, Phys. Rev. Lett. **120**, 120501 (2018).
[18] Y. E. Kraus, Y. Lahini, Z. Ringel, M. Verbin, and O. Zilberberg, Phys. Rev. Lett. **109**, 106402 (2012).
[19] O. Zilberberg, S. Huang, J. Guglielmon, M. Wang, K. P. Chen, Y. E. Kraus, and M. C. Rechtsman, Nature (London) **553**, 59 (2018).
[20] M. Lohse, C. Schweizer, H. M. Price, O. Zilberberg, and I. Bloch, Nature (London) **553**, 55 (2018).
[21] M. Verbin, O. Zilberberg, Y. Lahini, Y. E. Kraus, and Y. Silberberg, Phys. Rev. B **91**, 064201 (2015).
[22] E. Riva, M. I. N. Rosa, and M. Ruzzene, Phys. Rev. B **101**, 094307 (2020).
[23] I. Petrides, H. M. Price, and O. Zilberberg, Phys. Rev. B **98**, 125431 (2018).
[24] L. Privitera, A. Russomanno, R. Citro, and G. E. Santoro, Phys. Rev. Lett. **120**, 106601 (2018).
[25] P. G. Harper, Proc. Phys. Soc. London Sect. A **68**, 879 (1955).
[26] Z.-G. Chen, W. Zhu, Y. Tan, L. Wang, and G. Ma, arxiv: 1912.10267.
[27] L. D. Landau and E. M. Lifshitz, *Quantum Mechanics: Non-Relativistic Theory* (Elsevier Science, New York, 1991).
[28] E. Riva, V. Casieri, F. Resta, and F. Braghin, Phys. Rev. B **102**, 014305 (2020).
[29] S. Longhi, G. L. Giorgi, and R. Zambrini, Adv. Quantum Technol. **2**, 1800090 (2019).
[30] B. Zhou, H.-Z. Lu, R.-L. Chu, S.-Q. Shen, and Q. Niu, Phys. Rev. Lett. **101**, 246807 (2008).
[31] Y.-X. Xiao, G. Ma, Z.-Q. Zhang, and C. T. Chan, Phys. Rev. Lett. **118**, 166803 (2017).
[32] Z.-G. Chen, L. Wang, G. Zhang, and G. Ma, Phys. Rev. Applied **14**, 024023 (2020).
[33] Y.-X. Shen, Y.-G. Peng, D.-G. Zhao, X.-C. Chen, J. Zhu, and X.-F. Zhu, Phys. Rev. Lett. **122**, 094501 (2019).
[34] Y. Long and J. Ren, J. Acoust. Soc. Am. **146**, 742 (2019).
[35] See Supplemental Material at http://link.aps.org/supplemental/10.1103/PhysRevLett.126.054301 for more theoretical and simulation details, the topological states transfer in the system with waveguides, robustness discussion, and a video file of numerical demonstration.
[36] A. C. Vutha, Eur. J. Phys. **31**, 389 (2010).
[37] S. N. Shevchenko, S. Ashhab, and F. Nori, Phys. Rep. **492**, 1 (2010).
[38] J. Doppler, A. A. Mailybaev, J. Böhm, U. Kuhl, A. Girschik, F. Libisch, T. J. Milburn, P. Rabl, N. Moiseyev, and S. Rotter, Nature (London) **537**, 76 (2016).
[39] M. Heinrich, M.-A. Miri, S. Stützer, R. El-Ganainy, S. Nolte, A. Szameit, and D. N. Christodoulides, Nat. Commun. **5**, 3698 (2014).